Photons and Photocatalysts as limiting reagents for PET-RAFT photopolymerization

Bryan Parnitzke [a], Tochukwu Nwoko [a], Kate G. E. Bradford [a], Nethmi De Alwis Watuthanthrige,[a] Kevin Yehl,[a] Cyrille Boyer,[b] Dominik Konkolewicz [a,*]

Correspondence: d.konkolewicz@miamiOH.edu

Department of Chemistry and Biochemistry, Miami University, 651 E High St. Oxford, OH, 45056, USA

Centre for Advanced Macromolecular Design, School of Chemical Engineering, The University of New South Wales, UNSW Sydney NSW 2052, Australia

Abstract

The kinetics of photoinduced electron/energy transfer - reversible addition fragmentation chain transfer (PET-RAFT) polymerization were investigated using a model system of methyl acrylate (MA) in the presence of trithiocarbonate chain transfer agents and tris(2-phenylpyridine)iridium(III) ($Ir(ppy)_3$) as the photocatalyst. A powerful polymerization through oxygen approach was developed. Efficient PET-RAFT occurred under blue, violet, and green light with catalyst loadings of 10 ppm. Minimal polymerization was observed under orange or red light. Kinetic scaling analysis was developed to evaluate the impact of light intensity, catalyst loading and geometry of both the light source and the reaction vessel. A universal scaling law was developed for $Ir(ppy)_3$ catalyzed PET-RAFT, allowing both polymerization through oxygen and deoxygenated systems from the literature to be described across a range of light intensities, reaction conditions and geometries. Finally, the scaling analysis indicates that PET-RAFT

systems should be subject to less retardation than conventional RAFT systems, due to the chain transfer agent being involved in radical generation steps.

Introduction

Photochemistry has seen substantial growth over the past decade[1–3], with recent work highlighting the unique potential for light driven reactions to give well defined products under mild reaction conditions[4–8]. In particular, organic and polymer photochemistry has received significant attention due to the ability to perform otherwise challenging reactions[9–11], and the spatiotemporal control afforded by light driven reactions[12–15]. A critical aspect of photochemistry is the use of photons to drive the reaction forward, and chromophores to absorb the photons, and commence the chemical reactions[16–18]. However, other factors such as reaction vessel geometry, light source and reaction mode can also potentially impact the outcome of photochemical processes[19,20].

Among polymerization methods[21,22], reversible deactivation radical polymerization (RDRP) methods have emerged as powerful approaches for synthesizing polymers with good control over molecular weight[23] and polymer architectures, comparable to traditional living anionic polymerization, with control over tolerance to functional groups similar to conventional radical polymerization[24–27]. The two most used RDRP methods are atom transfer radical polymerization (ATRP) and reversible addition-fragmentation chain transfer (RAFT)[27–29]. Photochemically driven ATRP and RAFT methods have been developed in the past decade[30–32]. In particular, photoinduced electron/energy transfer - reversible addition fragmentation chain transfer (PET-RAFT) has emerged as a powerful tool for the synthesis of polymers with well-defined architecture for a wide variety of functional monomers[6,33,34].

PET-RAFT uses a photocatalyst[35–38] to promote and accelerate RAFT polymerization under mild conditions[2,39,40]. Hence, this technique has been used in several applications such as bioconjugates, 3D printing, polymer self-assembly, complex polymer formation, and photolithography[41–44]. In PET-RAFT the photocatalyst absorbs a photon, interacting with the RAFT chain transfer agent (CTA) through either an energy or electron transfer process, generating a propagating radical from the chain transfer agent[6,45–48]. The propagating radical can add monomer[49], terminate, or enter the RAFT degenerative transfer equilibrium[47,50,51]. One of the most widely used photocatalysts is tris(2-phenylpyridine)iridium(III) ($Ir(ppy)_3$) in both photochemically driven ATRP and PET-RAFT[6,52–54]. In PET-RAFT, the experimental evidence strongly suggests that $Ir(ppy)_3$ activates the CTA through an energy transfer pathway[55]. This is demonstrated in Scheme 1A, where PC represents the $Ir(ppy)_3$ photocatalyst. In earlier work, the single-factor impact of photoreactor design and reaction conditions were explored in the PET-RAFT of methyl acrylate (MA) controlled by trithiocarbonate CTAs under rigorously deoxygenated conditions[56]. Negligible polymerization was observed without rigorous deoxygenation, and no global analysis of reaction conditions on polymerization rate was performed [56]. However, with the rise of oxygen tolerant RAFT processes[57], including reactions that are run to polymerize through oxygen by reacting residual O_2 with propagating radicals[58]. One approach to facilitate this polymerization through oxygen is to essentially exclude air, by filling the reaction vessel until there is no gas either with reaction mixtures, or an immiscible inert solvent[59,60]. For downstream applications, especially at larger scale where rigorous deoxygenation is not feasible, PET-RAFT processes that are oxygen tolerant are especially important.

Despite the recent efforts in understanding PET-RAFT processes,[61,62] a universal relationship dependence of reaction rate on light source characteristics, geometric and surface to volume properties of the reaction vessel and reactant concentrations is lacking. Such a relationship would greatly facilitate subsequent innovations and applications of PET-RAFT, since the current individual studies generally give results that cannot be directly compared to each other. Further, comprehensive studies where key reaction parameters are simultaneously varied (wavelength, intensity, catalyst loading) are lacking, especially for the easier to implement polymerization through oxygen approaches[1]. Even where individual reaction and reactor parameters were investigated[56], global analysis factoring in surface to volume and photon counts were not explicitly considered.

In this work, the impact of reaction parameters, in particular, wavelength of light, reaction vessel diameter, photoreactor intensity and catalyst loading are comprehensively explored for the PET-RAFT of MA catalyzed by $Ir(ppy)_3$ under polymerization through oxygen conditions. A global analysis of the impact of reactor area to volume, photochemical source and intensity and catalyst loading is performed, showing a common behavior of these PET-RAFT reactions, and related energy transfer systems. This implies that rational design of PET-RAFT reactions under energy transfer conditions can be performed using known reagent concentrations, geometric considerations and light intensity. A key conclusion of these analyses is that under the studied conditions, relevant to many laboratory and approaching scale-up reactions, PET-RAFT is limited by the photocatalyst and light intensity. Increases in either parameter enhance the polymerization rate without loss of control.

Experimental Methods

Materials

All reagents were obtained from commercial suppliers unless otherwise stated.

Synthesis of 2-(((dodecylthio)carbonothioyl)thio)propanoic acid (PADTC)

2-(((Dodecylthio)carbonothioyl)thio)propanoic acid (PADTC) was synthesized as follows following a procedure outlined in the literature[63]: To a reaction flask, dodecanethiol (56.25 g, 278 mmol), tetramethylammonium bromide (3.55 g, 23.09 mmol), and 900 mL of acetone was added, stirring until solvated. 112.5 mL of 2.5 M NaOH was added dropwise. The mixture was stirred for 15 minutes, and the reaction flask was cooled completely over an ice bath. Simultaneously CS_2 (17.1 g, 225 mmol) was added over 15 minutes. The solution was left to stir for 30 minutes. Following, 2-bromopropanoic acid (43 mg, 280 mmol) was added dropwise. The flask was left uncapped, at 20 °C to stir overnight. 1 M HCl was added until the mixture was clear in color as crystallization occurs. The product was isolated and purified by recrystallization from hexane giving yellow crystals.

Polymerization Reaction Mixture Preparation. A 1.0 mL, *10 ppm catalyst*, reaction solution was created as follows: 1 mL methyl acrylate (0.95 g, 11 mmol), 0.039 g PADTC (0.11 mmol), 0.927 mL DMSO, and 0.072 mL $Ir(ppy)_3$, taken from a 1000 ppm stock solution in DMSO.

A 1.0 mL, *5 ppm catalyst*, reaction solution was created as follows: 1 mL methyl acrylate (0.95 g, 11 mmol), 0.039 g PADTC (0.11 mmol), 0.964 mL DMSO, and 0.036 mL $Ir(ppy)_3$, taken from a 1000 ppm stock solution in DMSO.

A 1.0 mL, *2 ppm catalyst*, reaction solution was created as follows: 1 mL methyl acrylate (0.95 g, 11 mmol), 0.039 g PADTC (0.11 mmol), 0.985 mL DMSO, and 0.014 mL $Ir(ppy)_3$, taken from a 1000 ppm stock solution in DMSO.

A 1.0 mL, *1 ppm catalyst*, reaction solution was created as follows: 1 mL methyl acrylate (0.95 g, 11 mmol), 0.039 g PADTC (0.11 mmol), 0.992 mL DMSO, and 0.007 mL $Ir(ppy)_3$, taken from a 1000 ppm stock solution in DMSO.

Table 1: Preparation of Polymerization mixtures

Solution	$Ir(ppy)_3$ volume from 1000 ppm stock (mL)	PADTC weight (g)	MA volume (mL)	DMSO volume (mL)
10 ppm	0.072	0.039	1.00	0.927
5 ppm	0.036	0.039	1.00	0.964
2 ppm	0.014	0.039	1.00	0.985
1 ppm	0.007	0.039	1.00	0.992

Typical Polymerization of Methyl Acrylate. A 4 mL glass vial containing a stir bar and 2.0 mL of the previously prepared solution was added, as outlined in **Polymerization Reaction Mixture Preparation**. The vial was filled with about 2.6 mL of mineral oil and placed in the corresponding cylindrical or flat photoreactor, violet (392 ± 8 nm), blue (450 ± 10 nm), green (510 ± 20 nm), orange (591 ± 7 nm), or red (634 ± 9 nm). All photoreactors were covered with aluminum foil and the reaction vials were stirred for 120 minutes with aliquots taken for NMR and SEC analysis. Samples with monomer conversion greater than or equal to 35% were prepared and analyzed by SEC to give molecular weight and dispersity data.

The diameter of the vial system was changed to see the effects it has on polymerization. Under blue light, 2 mL of 10 ppm reaction solution was added to a 20 mL vial (25 nm), a 15 mL vial (14.5 nm), and a 4 mL vial (12.5 nm).

Scale-Up Experiment in a 50 mL round bottom flask. A scaled-up experiment was developed adapting the conditions used in the 2mL vial experiments. Briefly, the reaction mixture was prepared using 24.6 mL of methyl acrylate (23.75 g, 0.2758 mol), PADTC (0.9672 g, 2.759 mmol) and $Ir(ppy)_3$ (1.8 mg, 2.7 µmol) taken from the 1000 ppm $Ir(ppy)_3$ stock solution were combined with 23.175 mL of DMSO in a 50 mL round bottom flask equipped with a magnetic stirrer. The reaction flask was topped off with mineral oil and capped with a rubber septum. The reaction mixture was irradiated using a flat blue light photoreactor with samples taken periodically and analyzed by NMR for conversion data and SEC to give molecular weight and dispersity data.

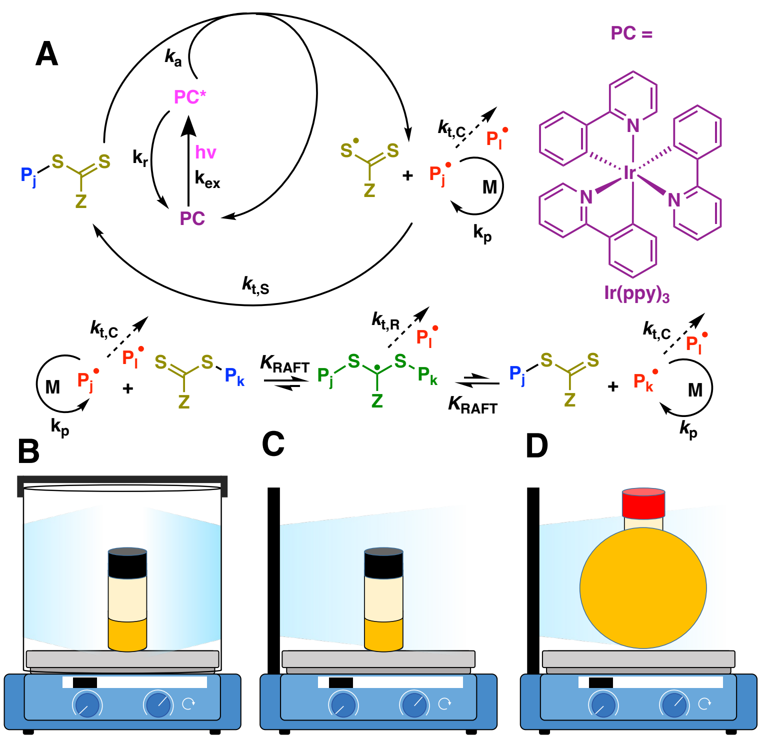

Scheme 1. A) Proposed mechanism of the $Ir(ppy)_3$ catalyzed PET-RAFT polymerization of MA. B) schematic diagram of the cylindrical light source/photoreactor with a cylindrical reaction vessel setup. C) schematic diagram of the flat light source/photoreactor with a cylindrical reaction vessel setup D) schematic diagram of the flat light source/photoreactor with a spherical

reaction vessel setup. All set ups shown, which includes the reaction vessels filled with reaction mixture and oil, were placed inside of an aluminum foil-covered photoreactor on a stir plate.

Results and Discussion

In earlier work[56], rigorously deoxygenated conditions were considered, whereas here, a polymerization was carried out in the presence of oxygen. Parameters to be investigated are the wavelength of light used, the aspect ratio of the cylindrical reaction vessel, geometry of the light source and reaction vessel, light intensity, and the photocatalyst loading. The proposed mechanism of PET-RAFT using $Ir(ppy)_3$ as the photocatalyst (PC) is given in Scheme 1A. In particular, the energy transfer mechanism has been shown to dominate for $Ir(ppy)_3$[55], as indicated by the homolytic cleavage of the C-S bond of the CTA. The UV-Visible (UV-Vis) spectra of both $Ir(ppy)_3$ and PADTC are given in Figure S1, indicating strong absorption by the $Ir(ppy)_3$ photocatalyst in both the violet and blue regions of the visible spectrum, moderate absorbance in the green, and minimal absorbance in the yellow, orange or red.

The proposed mechanism proceeds with photon absorption by the PC, with rate coefficient k_{ex}, followed by energy transfer between PC* and the CTA, with rate coefficient k_a. To confirm that CTA interacts efficiently with the excited state photocatalyst, Stern-Volmer analysis was performed as outlined in Figure S2. The Stern-Volmer analysis suggests a highly efficient reaction between the excited state photocatalyst and the CTA, giving $k_a \sim 2 \times 10^9$ M^{-1} s^{-1}. This is assuming that all quenching of the excited state photocatalyst by the CTA occurs through k_a. It is also possible that some energy transfer events from the excited state PC to the CTA lead to relaxation of the excited state CTA rather than bond homolysis. This makes the rate coefficient for radical generation by quenching the excited state PC substantially smaller than the measured quenching rate coefficient.

The excited state photocatalyst can also return to the ground state without excitation of the CTA with rate coefficient k_r. The propagating radical can add monomer with rate coefficient k_p, undergo conventional radical termination with rate coefficient k_{tC}, or recombine with the thiocarbonylthiyl radical from the CTA with rate coefficient k_{tS}. Control over the polymerization is gained primarily through the RAFT equilibrium, with equilibrium constant K_{RAFT}, and the intermediate radical can cross terminate with propagating radicals with rate coefficient k_{tR}.

Initially, the effects of the wavelength of light on the photocatalyzed polymerization was explored as indicated in Figure 1. Photophysical properties of the photoreactors, the photocatalyst $Ir(ppy)_3$ and the chain transfer agent, PADTC, were given in Figures S1-S4. Importantly, Figure S4 indicate that negligible photodegradation occurs due to extended exposure of either $Ir(ppy)_3$ or PADTC to high energy violet and blue light.

Initially cylindrical reaction vessels in a cylindrical photoreactor were explored as shown in Scheme 1B. Figure 1A indicates that the kinetics of PET-RAFT polymerization using 10 ppm of $Ir(ppy)_3$ photocatalyst are dependent on the wavelength. The lowest wavelength of visible light studied, violet, has the highest rate of polymerization. Increasing the wavelengths of the LED in photoreactor from violet to blue and green led to a gradual reduction in polymerization rate. As expected, the photoreactors containing LEDs emitting long wavelength orange and red photons gave negligible polymerization rates, due to very low extinction coefficients in the orange/red regions of the $Ir(ppy)_3$ absorbance spectrum. All systems had some small induction period, which is consistent with the polymerization through oxygen. It is noteworthy that except orange all photoreactors had similar intensities in the order of 4-8 mW/cm^2. Due to the relatively narrow range of wavelengths similar photoreactor intensities correlate with similar photon flux through the sample. Therefore, the differences are attributed to spectral overlap between the photoreactor and the $Ir(ppy)_3$, with violet and blue having substantially better spectral overlap than green, and orange and red having poor spectral overlap (SI, Figures S1, Table S1 Figure S3). Similar results were observed at 5 ppm loading of $Ir(ppy)_3$, although the reaction tended to be slower, as seen in SI, Figure S5A.

Figure 1B displays the evolution of number averaged molecular weight (M_n) and dispersity (M_w/M_n) with monomer conversion. The PET-RAFT polymerization of methyl acrylate yields polymers of low dispersity of ~1.1-1.2. Additionally, the M_n increases linearly with monomer conversion, with good agreement between the experimental and theoretical M_n values ($M_{n\text{-}Th}$). The linear evolution of M_n with monomer conversion and low dispersity were observed of both the 10 ppm loading of $Ir(ppy)_3$ shown in Figure 1B and 5 ppm of photocatalyst given in SI, Figure S5B. In general, the experimental M_n was slightly higher than the theoretical M_n possibly due to the polymerization through oxygen approach terminating a small fraction of chains prematurely.

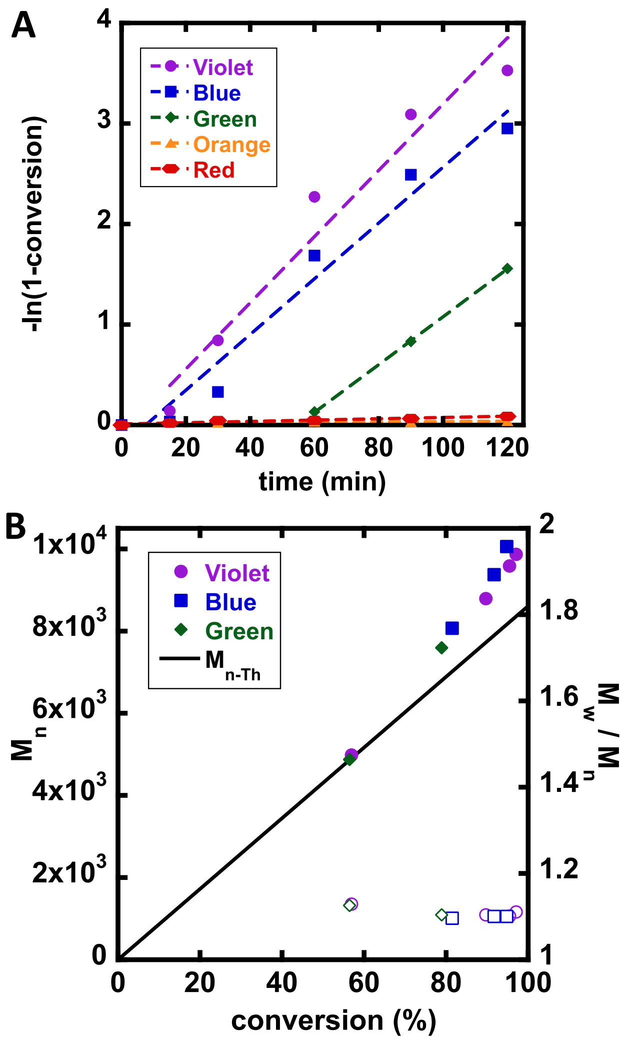

Figure 1. Rates of PET-RAFT polymerization of MA under wavelengths of light with conditions of [MA]:[PADTC], 100:1, and 10 ppm photocatalyst. A) Kinetics of polymerization under violet (399 ± 8 nm, 5.4 ± 0.2 mW/cm^2), blue (450 ± 10 nm, 5.4 ± 0.2 mW/cm^2), green (510 nm ± 20, 6.4 ± 0.5 mW/cm^2), orange (591 ± 7 nm, 1.1 ± 0.1 mW/cm^2), and red (630 ± 10 nm, 4.6 ± 0.5 mW/cm^2) light. B) Evolution of M_n (solid points) and M_w/M_n (hollow points) with MA polymerization performed under violet, blue, and green light. The solid line represents the theoretical M_n values.

In earlier work, the effect of photoreactor dimensions and volumes was found to be of low significance when considering well deoxygenated systems. In particular, changing the volume of the reaction mixture in a cylindrical reaction vessel led to minimal changes in reaction rate since a proportionally larger surface area was exposed by this approach. However, using a polymerization through oxygen approach here may not follow the same trend since the fraction of residual oxygen may change with the volume of the flask occupied by the reaction mixture. The kinetics of 2 mL reaction volume systems were measured with varying vial diameters as shown in Figure 2A. The 12.5 mm diameter (4 mL reaction vessel) vial had the highest rate, with the rate of reaction decreasing as the vial diameter increased. The reaction in a flask of diameter 14.5 mm (15 mL reaction vessel) was notably slower than the 12.5 mm vial, and the 25 mm (20 mL reaction vessel) barely reached 20% monomer conversion. The most likely reason for this is that the 4 mL vial had 50% of its volume occupied by reaction mixture and the remaining 50% occupied by inert mineral oil. In contrast, the 15 mL vial had 13% of its volume occupied by the reaction mixture, and the 20 mL vial had just 10% of the vessel occupied by the reaction mixture. Further, the small surface area of exposed reaction mixture in the 20 mL vial compared to the 15 mL vial (25 mm *vs* 14.5 mm) could lead to inefficient photon capture. This is a notable result, and in contrast to earlier work, with the main reasons being the polymerization through oxygen approach and the wider range of reaction vessel diameters used here[56]. Figure 2B indicates that all polymers have linear evolution of M_n conversion and good agreement between theoretical and experimental values. Additionally, all polymers had low dispersity, indicating that the diameter of the vial primarily impacts the kinetics of the PET-RAFT polymerization rather than the properties of the synthesized polymers at a given monomer conversion.

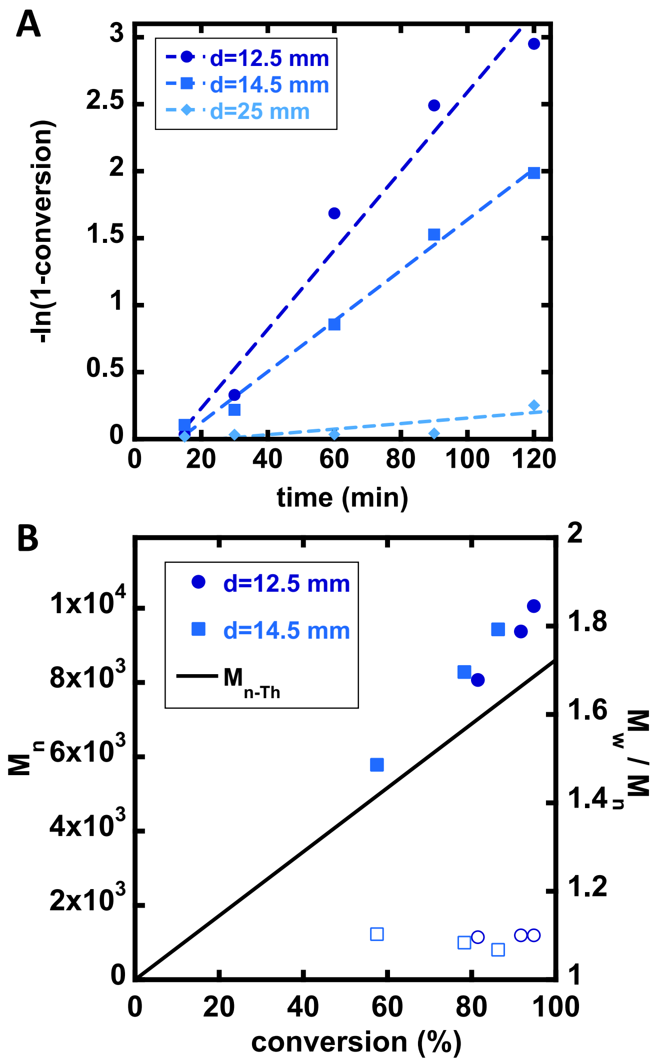

Figure 2. Rate of PET-RAFT polymerization of MA under blue light with conditions of [MA]:[PADTC], 100:1, and 10 ppm photocatalyst. A) Kinetics of polymerization under blue (450 ± 10 nm, Intensity 5.3 ± 0.2 mW/cm^2) light. B) Plot of M_n and M_w/M_n as MA polymerization progresses in 12.5 mm and 14.5 mm vials. The solid line shows where M_n theoretically should be throughout the polymerization.

Since PET-RAFT is a photochemically driven process, it is essential to study the impact of light intensity on the outcome of the reaction. In general, higher intensities of photocatalyst, of the same wavelength led to an increase in photon flux within the system, which should accelerate the photocatalytic processes. In prior work a ½ order dependence of polymerization rate on light intensity was determined[56,64,65]. As seen in Figure 3A, higher intensity blue photoreactors led to higher polymerization rates. The dependence of apparent polymerization rate ($k_{p,}^{app}$, taken as the slope of the semilogarithmic plot) scaled as with the 0.5 order of photoreactor intensity. It is also important to note that this polymerization through oxygen strategy led to longer induction periods with lower light intensity, consistent with the slower rate of radical generation needed to consume residual oxygen, as well as the formation of singlet oxygen[66]. Similar trends were observed with 10 ppm catalyst (Figure S6), except it appears the system had minimal increase at higher intensity. This could be due to some small extent of photocatalyst self-quenching[67–70], but the effect is minor. As anticipated, Figure 3B shows that all polymers are well controlled, with linear evolution of M_n with monomer conversion, close the theory line, and narrow molecular weight distributions. The slightly higher experimental M_n compared to the theoretical M_n could be due to termination of some chains in the polymerization through oxygen process.

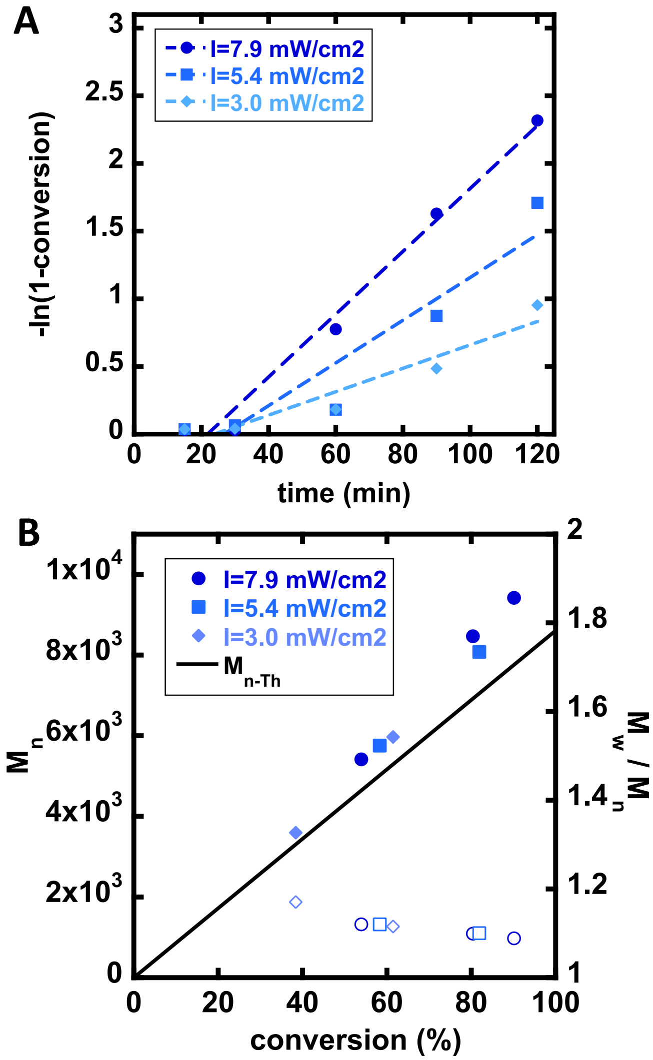

Figure 3. A) Kinetics of PET-RAFT polymerization of MA under conditions of [MA]:[PADTC], 100:1, and 5 ppm photocatalyst with blue light (450 ± 10 nm, with Intensity of 7.9 ± 0.4, 5.4 ± 0.2, or 3.0 ± 0.3 mW/cm^2) B) Plot of M_n and M_w/M_n as MA polymerization progresses under blue light of different intensities. The solid line shows where M_n theoretically should be throughout the polymerization.

In PET-RAFT, the photocatalyst has a unique role in initiating and driving the reaction. Therefore, the complex relationship between reaction rate and catalyst loading was explored.

Due to the radical process, involving both radical generation through photocatalysis and radical loss through termination pathways, a non-linear relationship between photocatalyst loading and reaction rate is anticipated[56]. Figure 4A displays the correlation found using blue light, where a higher concentration of the $Ir(ppy)_3$ photocatalyst yields a higher rate, respectively decreasing with lower concentrations. This trend is consistent with earlier work, where reactions were rigorously deoxygenated[56]. However, the decrease in polymerization rate coupled with a long induction period was observed at 1 ppm catalyst loading. The most likely reason for this is the presence of oxygen. The 1 ppm catalyst loading is too low for the efficient removal of oxygen, causing a longer inhibition period, causing insufficient polymerization through oxygen. This is consistent with the induction period increasing with lower catalyst loading in general for Figure 4A. However, the synthesized polymers were well controlled for all employed catalyst loadings, which gave conversion above 30%. The evolution of M_n was linear and closed to the theory line, with dispersities in the range of 1.1-1.2 as seen in Figure 4B.

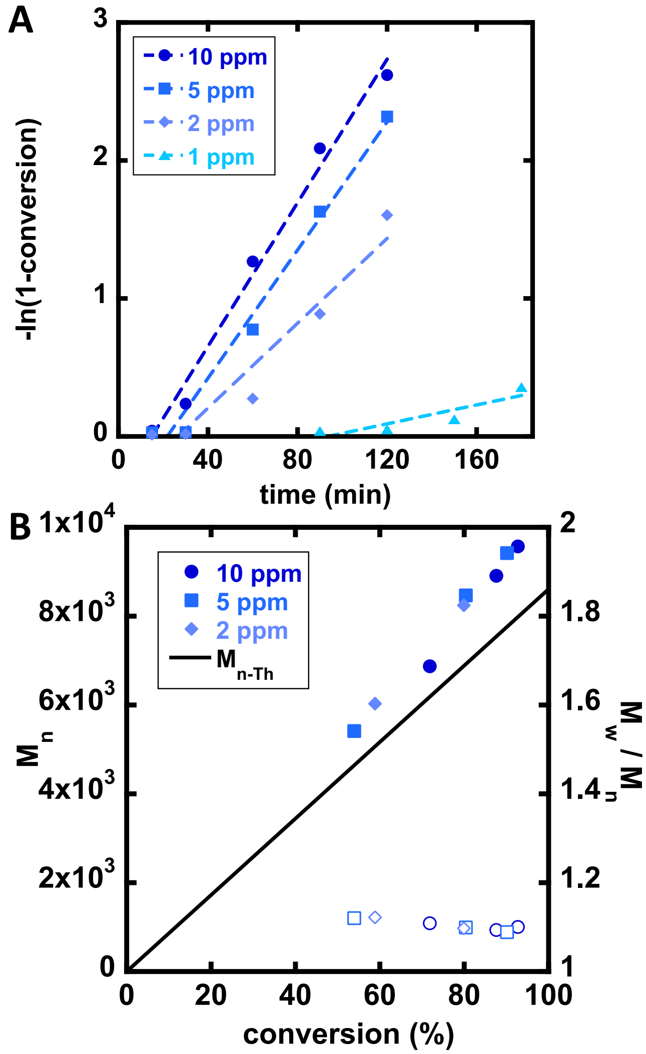

Figure 4. A) Rates of PET-RAFT polymerization of MA under blue light (450 ± 10 nm, 7.9 ± 0.4 mW/cm^2) with conditions of [MA]:[PADTC], 100:1, and varying concentrations of the $Ir(ppy)_3$ photocatalyst. B) Plot of M_n and M_w/M_n as MA polymerization progresses under blue light of different intensities. The solid line shows where M_n theoretically should be throughout the polymerization.

Under green light, the same trends in reaction rate with photocatalyst are observed in Figure S7A, where 10 ppm yielded the greatest rate followed by 5 ppm. The mixture with 2 ppm catalyst loading simply had a very slow and negligible amount of polymerization occurred over time. Under green light, a significant drop in the rate of the polymerization occurred between 10 and 5 ppm catalyst loading, which is comparable to the drop between 2 and 1 ppm loading under blue light. The likely reason for the higher required catalyst loading for the polymerization under green light is that the $Ir(ppy)_3$ photocatalyst displays a stronger absorption under blue light compared to green light. Therefore, a higher catalyst loading is required for the effective excitation of the photocatalyst and the polymerization through oxygen.

To further explore the impact of reactor geometries and reaction conditions two additional geometries were considered. One involved a flat light source and a cylindrical reaction vessel as demonstrated in Scheme 1C, and finally a larger scale spherical reaction vessel with a flat light source was used as given in Scheme 1D. As seen in Figure 5A the flat light source/cylindrical reaction vessel leads to efficient photochemical reactions with evidence of mild retardation occurring at higher CTA loadings, corresponding to shorter target molecular weights. The inset of Figure 5A indicates a linear relationship between k_p^{app} and $[CTA]^{-0.25}$. Further, Figure S8 indicates that lower photocatalyst loadings lead to slower polymerization rates in the flat light source, cylindrical reaction vessel geometry. This is consistent with the results of Figure 4A. The overall scaling of k_p^{app} with reaction conditions is investigated subsequently. As indicated in Figure 5B all polymerization conditions led to well controlled polymers with the final molecular weight distribution being narrow and in good agreement with the theoretical M_n.

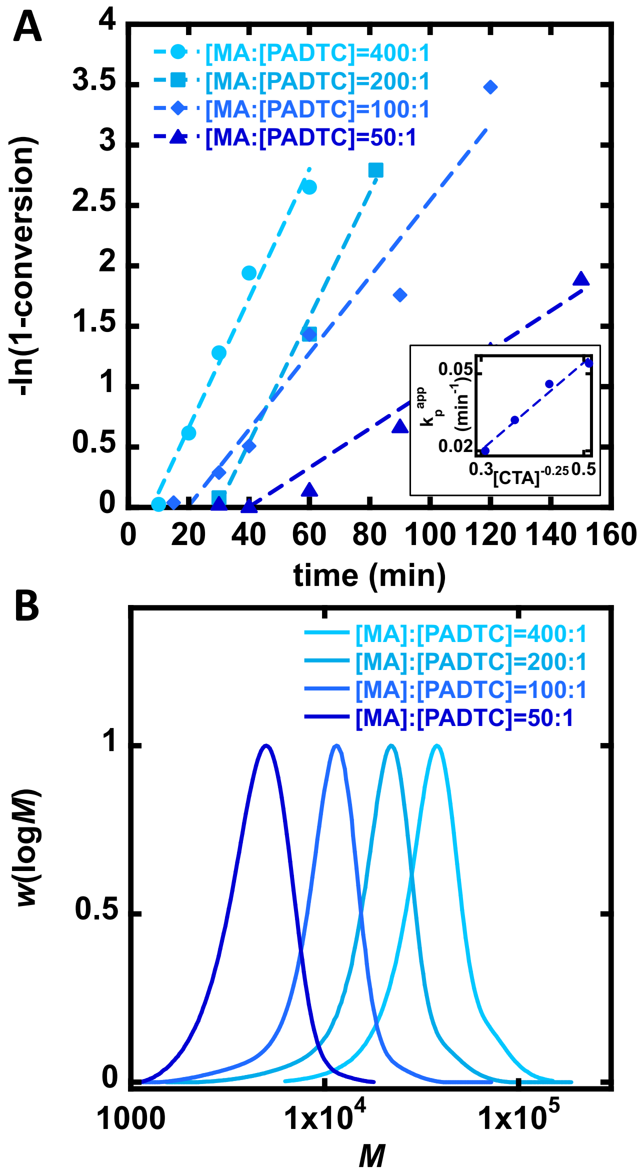

Figure 5. A) Rates of PET-RAFT polymerization of MA under blue light (450 ± 10 nm, 12.7 ± 0.6 mW/cm^2) with 10 ppm of $Ir(ppy)_3$ photocatalyst, and varying concentrations of PADTC using a flat light source and a cylindrical reaction vessel. Inset gives scaling of k_p^{app} vs $[CTA]^{-0.25}$ B) Final molecular weight distributions of polymers synthesized.

Finally, a larger scale reaction was performed. The experiments performed in the study so far focus on laboratory scale reactions in the order of 2 mL of reaction solution. Finally, a 50 mL round bottom flask, approximated as a sphere of radius 2.28 cm was used in conjunction with the flat light source. As seen in Figure 6A, the spherical system at substantially larger scale of 50 mL gave comparable, albeit slightly slower, reaction kinetics than the 2 mL reaction systems in cylindrical reaction vessels. The inset of Figure 6A shows the reaction set up. All systems used no deoxygenation, but rather minimized oxygen by filling the reaction vessel fully with mineral oil. The fastest reaction occurred with the highest intensity light source (flat blue LED) with 2 mL reaction volume in a cylindrical vessel, followed by the 2 mL reaction using the cylindrical light source, with the scaled-up system of 50 mL reaction volume with a flat light source being the slowest. As seen in Figure 6B, all polymerizations led to well defined molecular weight distributions centered near the target molecular weight of ~8500. The competing factors of reaction scale, light intensity and exposed surface area of the reaction vessel necessitate a detailed mathematical analysis to quantitatively predict and describe the impact of each of these parameters. This is especially true for potential downstream applications which will likely vary several parameters from those outlined in this study.

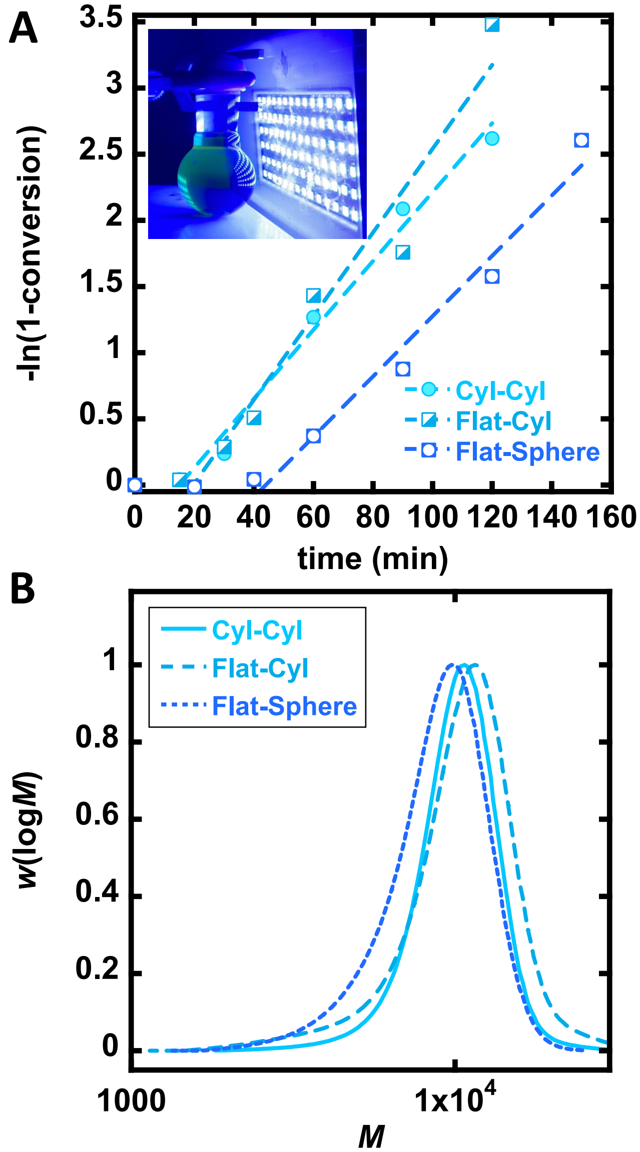

Figure 6. A) Rates of PET-RAFT polymerization of MA under blue light (450 ± 10 nm) Using either a flat light source (Intensity = 12.7 ± 0.6 mW/cm^2) or Cylindrical light source (Intensity = 7.9 ± 0.4 mW/cm^2). Polymerization under the conditions [MA]:[PADTC] = 100:1, 10 ppm of Ir(ppy)$_3$ photocatalyst using 2 mL of reaction volume in a 12.5 mm cylinder or a. 22.8 mm spherical reaction vessel. Inset gives reaction set up for 50 mL flat-sphere reaction B) Final molecular weight distributions of polymers synthesized.

In prior literature work a single reaction condition variation was discussed,[56] and how this impacts the polymerization rate. Similarly, within this study, control over the polymerization was generally good, with narrow molecular weight distributions and linear evolution of M_n with conversion. However, the single factor variation in Figures 1-5, or in prior work, will not fully capture all behaviors as different photoreactor intensity and catalyst loadings were used. This is especially important when applying PET-RAFT in other laboratories, as the intensity of the light source, and exact reaction vessels may differ from those used here. Figure 7A plots the combinatorial effects of catalyst loading and photoreactor intensity for PET-RAFT of MA under blue light irradiation in cylindrical reactors using cylindrical light sources. The general trend in Figure 7A is that higher catalyst loading or higher intensity photoreactors led to increases in polymerization rate. This is consistent with the photon flux and photocatalyst loading being the limiting reagents in PET-RAFT reactions, hence increases in either, generally lead to increases in reaction rates. In particular, there is a critical light intensity and catalyst concentration needed to achieve reasonable polymerization rates in this polymerization through oxygen approach. Increases in either parameter alone, within the range studied here, can lead to notable improvements in reaction rate, as the residual oxygen is effectively removed.

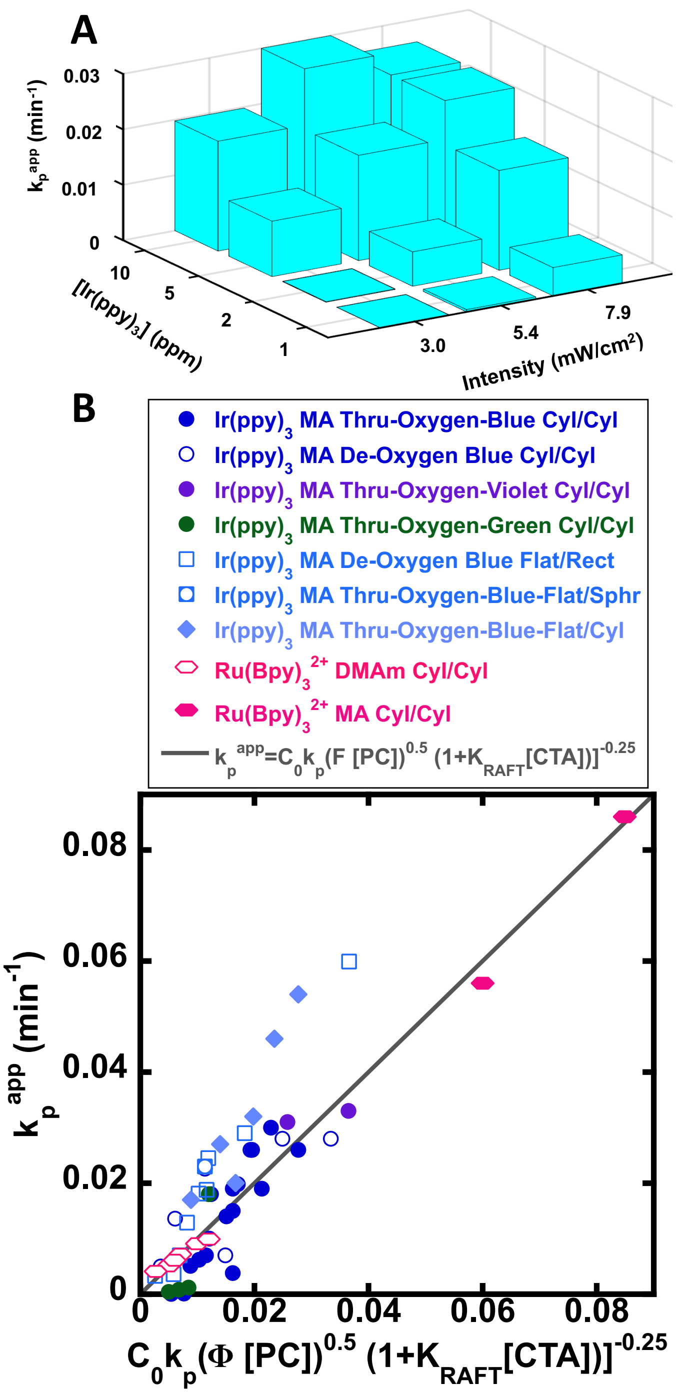

Figure 7. A) 3D plot, showing the effect of light intensity and catalyst loading on the polymerization kinetics ($k_{p,}{}^{app}$) of the PET-RAFT of MA under the conditions [MA]:[PADTC]=100:1, with 50 vol% monomer in DMSO. B) Scaling analysis of Eq 2 for a variety of $Ir(ppy)_3$ catalyzed PET-RAFT polymerizations of MA and $Ru(bpy)_3^{2+}$ catalyzed PET-

RAFT polymerizations of MA[71] or N-Ndimethylacrylamide.[71,72] Hollow symbols represent deoxygenated systems and solid represent polymerization through oxygen. Round symbols represent cylindrical geometry, and square symbols represent rectangular geometry. K_{RAFT} taken to be 10^3 M^{-1} for MA with trithiocarbonate CTA.

In analyzing the sum of all data presented here, a scaling analysis was performed to identify if a universal relationship exists between the various reaction conditions, both from this work, and also from our earlier systematic study[56]. In radical polymerization, the rate of the reaction is proportional to the propagating radical concentration [P•]. As outlined in the supporting information, a universal scaling relationship for PET-RAFT through the energy transfer mechanism, which applies to $Ir(ppy)_3$ and also $Ru(bpy)_3^{2+}$ photocatalysts,[55] has been derived. Applying the mechanism in Scheme 1A and using the steady state approximations in the radical and excited state photocatalyst concentration gives a predicted scaling law between reaction parameters and observed polymerization rates.

Given the near linearity of plot of $\ln[M]_0/[M]$, vs time in Figures 1-6 after any induction period, the slope of these kinetic semilogarithmic plots is denoted k_p^{app} and is related to the propagating radical concentration, [P•], though the relationship:

$$k_p^{app} = k_p[P^\bullet] \quad (1)$$

In general, linear or close to linear pseudo-first order kinetic plots were found across a range of polymerization conditions, reaction vessels and light sources. For downstream applications, high monomer conversion is important, hence the near linearity of the first order kinetic plot will likely facilitate eventual applications of PET-RAFT.

As outlined in the supporting information the [P•] is a function of the photon flux entering the reaction vessel per second, Φ, the photocatalyst concentration, [PC], the equilibrium constant of the RAFT reaction, K_{RAFT}, and CTA concentration [CTA], giving:

$$k_p^{app} = C_0\, k_p([PC]\Phi)^{1/2}\times(1 + K_{RAFT}[\mathrm{CTA}])^{-1/4} \tag{2}$$

Where C_0 is a constant for a given photocatalyst, CTA, monomer, and wavelength. Φ can generally be written as the density of photons entering the reaction vessel through exposed surface *A*, where the reactor has a volume *V* giving:

$$\Phi = \frac{I\times A}{E_\lambda N_A\times V} \tag{3}$$

Where *I* is the photoreactor intensity, N_A is Avogadro's number, and E_λ is the energy of one photon of wavelength λ in J, given by $E_\lambda=hc/\lambda$, where *h* is Planck's constant and *c* is the speed of light. The supporting information considers different combinations of light source and reaction vessel geometry facilitating a new and universal analysis across different batch photochemical reaction geometries.

The analysis in Eq 2 suggests that k_p^{app} should be a linear function of $([PC]\Phi)^{1/2}\times(1 + K_{RAFT}[\mathrm{CTA}])^{-1/4}$. Different wavelengths will give different values of C_0, as given in Table S2. As seen in Figure 7B, the general scaling relationship across over 45 experiments was established. Essentially, all experiments performed in either a flat or cylindrical light source, rectangular; cylindrical; or spherical reaction vessels, using trithiocarbonate RAFT agents and $Ir(ppy)_3$ or $Ru(bpy)_3^{2+}$can be combined onto a single scaling law. The kinetics of PET-RAFT catalyzed by $Ir(ppy)_3$ and $Ru(bpy)_3^{2+}$ photocatalysts were described using the same relationship, albeit distinct scaling factors C_0 were required, consistent with both these catalysts following the energy transfer mechanism. [55] In all MA polymerizations, a K_{RAFT} of 10^3 M^{-1} was used, which is consistent with trithiocarbonate mediated polymerization of acrylates[73].

The relationship in Figure 7B is a unique and powerful result that indicates that an energy-transfer PET-RAFT system can be predicted with knowledge of concentrations of reagents, photochemical reactor intensity, light source geometry, reaction vessel geometry, exposed surface area of reaction vessel and reaction volume, which is substantially more predictive than earlier work that simply focused on single factor variations developed earlier [56].

The key conclusion of equation 2 and Figure 7B is that in typical PET-RAFT reactions, the reaction rate is intimately tied to photocatalyst concentration and light intensity with both scaling as the ½ power. The analysis in Figure 7 also suggests that saturation is unlikely under lab conditions, and even larger scale reactions of 50 mL. Another key prediction of Eq 2 is that assuming intermediate radical termination PET-RAFT reactions are less retarded than their corresponding thermal RAFT processes. This is because the retardation in PET-RAFT scales as $(1 + K_{RAFT}[\mathrm{CTA}])^{-1/4} \sim [\mathrm{CTA}]^{-1/4}$ at high K_{RAFT} systems, where retardation is dominant. In contrast, thermal RAFT scales as $(1 + K_{RAFT}[\mathrm{CTA}])^{-1/2} \sim [\mathrm{CTA}]^{-1/2}$ in high K_{RAFT} systems[73]. Indeed, new analysis of previously published data of PET-RAFT as a function of CTA loading in Figure S9 indicates that the R^2 value of $k_p^{app} \propto [\mathrm{CTA}]^{-1/4}$ is superior to the previously published scaling law of $k_p^{app} \propto [\mathrm{CTA}]^{-1/2}$, also giving smaller residuals than the earlier published analysis [56]. These analyses further validate the newly developed scaling law presented in Eq 2.

The supporting information uses kinetic analysis compared to initial CTA loading ($[\mathrm{CTA}]_0$) to estimate the dead chain fraction as a function of propagating radical concertation, $[P^\bullet]$, and RAFT equilibrium constant, K_{RAFT}. Under typical polymerization conditions, $[P^\bullet] \sim 10^{-8}$ M, estimated from typical k_p^{app}, values in Table S3, and $K_{\mathrm{RAFT}}=10^3$ M^{-1},[73] the dead chain fraction is estimated to be in the order of 5%, as shown in Figure S10. This is because PET-RAFT initiation leads to radical generation, but control over polymer structure is primarily achieved through RAFT degenerative exchange.[74,75]

It is notable that both rigorously deoxygenated and polymerization through oxygen data follow the same general law, except those deoxygenated systems were often slightly above those that polymerize in the presence of oxygen. This could be due to oxygen-based inhibition, especially at the lower catalyst and light intensity systems indicated in Figure 7A. Overall the results in Figure 7B indicate that under typical PET-RAFT conditions, reactions are in a regime where both increases in photon intensity, and catalyst loading lead to meaningful increases in reaction rate. At very high catalyst loadings or large reaction volumes, saturation and even self-quenching are possible,[76] however, these conditions deviate from the typical ppm catalyst loadings used in PET-RAFT. Another important benefit of PET-RAFT over conventional RAFT, is that retardation is anticipated to be less significant in PET-RAFT than conventional RAFT due to the unique role of the CTA being involved in the radical generation step.

Conclusions

This work has investigated the detailed kinetics and properties of MA polymers made by PET-RAFT catalyzed by $Ir(ppy)_3$, using an efficient polymerization through oxygen approach. The results indicate that the typical lab scale, and scaled up PET-RAFT systems behave in a regime where both increases in light intensity and photocatalyst loading enhance polymerization rates, with both following a square root scaling law. Interestingly, scaling analysis also suggests that PET-RAFT processes may be less susceptible to retardation effects than conventional thermal reactions. Finally, a universal scaling law was developed for energy-transfer PET-RAFT reactions, based on photocatalyst loading, photon flux, reactor geometry and RAFT CTA loading. Within typical experimental ranges, a monotonic increase in reaction rate with photon flux and catalyst loading is expected. This allows a global description of a wide variety of PET-RAFT reactions, indicating the common mechanism dictating the reaction, and facilitates future applications of PET-RAFT.

Conflicts of Interest

The authors declare no competing interests

Acknowledgements

We are grateful to Dr. Hong Wang and Sachini Nishara Weerasinghe for experimental assistance. BP was supported through the National Science Foundation Research Experiences for Undergraduates (REU) program under award number CHE-1851795. This work was partially supported by the National Science Foundation under award number CHE-2203727 for scaling analysis and photophysical characterization. 400 MHz NMR Instrumentation at Miami University is supported by the National Science Foundation under award number CHE-1919850.

References

(1) Corrigan, N.; Yeow, J.; Judzewitsch, P.; Xu, J.; Boyer, C. Seeing the Light: Advancing Materials Chemistry through Photopolymerization. *Angewandte Chemie International Edition* **2019**, *58* (16), 5170–5189.

(2) Bellotti, V.; Simonutti, R. New Light in Polymer Science: Photoinduced Reversible Addition-Fragmentation Chain Transfer Polymerization (PET-RAFT) as Innovative Strategy for the Synthesis of Advanced Materials. *Polymers (Basel)* **2021**, *13* (7), 1119.

(3) Zhu, X.; Xu, Y.; Zhao, C.; Jia, C.; Guo, X. Recent Advances in Photochemical Reactions on Single-Molecule Electrical Platforms. *Macromol Rapid Commun* **2022**, 2200017.

(4) Ribelli, T. G.; Konkolewicz, D.; Bernhard, S.; Matyjaszewski, K. How Are Radicals (Re) Generated in Photochemical ATRP? *J Am Chem Soc* **2014**, *136* (38), 13303–13312.

(5) Amerik, Y.; Guillet, J. E. The Photochemistry of Ketone Polymers. IV. Photolysis of Methyl Vinyl Ketone Copolymers. *Macromolecules* **1971**, *4* (4), 375–379.

(6) Allegrezza, M. L.; Konkolewicz, D. PET-RAFT Polymerization: Mechanistic Perspectives for Future Materials. *ACS Macro Lett* **2021**, *10* (4), 433–446.

(7) Hiltebrandt, K.; Kaupp, M.; Molle, E.; Menzel, J. P.; Blinco, J. P.; Barner-Kowollik, C. Star Polymer Synthesis via λ-Orthogonal Photochemistry. *Chemical Communications* **2016**, *52* (60), 9426–9429.
(8) Delafresnaye, L.; Jung, K.; Boyer, C.; Barner-Kowollik, C. Two Colours of Light Drive PET–RAFT Photoligation. *Polym Chem* **2020**, *11* (40), 6453–6462.
(9) Fedynyshyn, T. H.; Kunz, R. R.; Sinta, R. F.; Goodman, R. B.; Doran, S. P. Polymer Photochemistry at Advanced Optical Wavelengths. *Journal of Vacuum Science & Technology B: Microelectronics and Nanometer Structures Processing, Measurement, and Phenomena* **2000**, *18* (6), 3332–3339.
(10) Smets, G. Organic Polymer Photochemistry. *Polym J* **1985**, *17* (1), 153–165.
(11) Zimmerman, H. E.; O'Brien, M. E. Photochemistry of Organic Molecules Entwined in Spiderwebs; the Use of Poly (Methyl Methacrylate) Glass for Restricting Excited-State Motion. *J Org Chem* **1994**, *59* (7), 1809–1816.
(12) Reeves, J. A.; de Alwis Watuthanthrige, N.; Boyer, C.; Konkolewicz, D. Intrinsic and Catalyzed Photochemistry of Phenylvinylketone for Wavelength-Sensitive Controlled Polymerization. *ChemPhotoChem* **2019**, *3* (11), 1171–1179.
(13) Chatani, S.; Kloxin, C. J.; Bowman, C. N. The Power of Light in Polymer Science: Photochemical Processes to Manipulate Polymer Formation, Structure, and Properties. *Polym Chem* **2014**, *5* (7), 2187–2201.
(14) Olson, R. A.; Korpusik, A. B.; Sumerlin, B. S. Enlightening Advances in Polymer Bioconjugate Chemistry: Light-Based Techniques for Grafting to and from Biomacromolecules. *Chem Sci* **2020**, *11* (20), 5142–5156.
(15) Seo, S. E.; Discekici, E. H.; Zhang, Y.; Bates, C. M.; Hawker, C. J. Surface-initiated PET-RAFT Polymerization under Metal-free and Ambient Conditions Using Enzyme Degassing. *Journal of Polymer Science* **2020**, *58* (1), 70–76.
(16) Burridge, K. M.; Wright, T. A.; Page, R. C.; Konkolewicz, D. Photochemistry for Well-Defined Polymers in Aqueous Media: From Fundamentals to Polymer Nanoparticles to Bioconjugates. *Macromol Rapid Commun* **2018**, *39* (12), 1800093.
(17) de Alwis Watuthanthrige, N.; Allegrezza, M. L.; Dolan, M. T.; Kloster, A. J.; Kovaliov, M.; Averick, S.; Konkolewicz, D. In-situ Chemiluminescence-Driven Reversible Addition–Fragmentation Chain-Transfer Photopolymerization. *Angewandte Chemie International Edition* **2019**, *58* (34), 11826–11829.
(18) Allegrezza, M. L.; DeMartini, Z. M.; Kloster, A. J.; Digby, Z. A.; Konkolewicz, D. Visible and Sunlight Driven RAFT Photopolymerization Accelerated by Amines: Kinetics and Mechanism. *Polym Chem* **2016**, *7* (43), 6626–6636.
(19) Sezen-Edmonds, M.; Tabora, J. E.; Cohen, B. M.; Zaretsky, S.; Simmons, E. M.; Sherwood, T. C.; Ramirez, A. Predicting Performance of Photochemical Transformations for Scaling up in Different Platforms by Combining High-Throughput Experimentation with Computational Modeling. *Org Process Res Dev* **2020**, *24* (10), 2128–2138.
(20) Su, Y.; Straathof, N. J. W.; Hessel, V.; Noel, T. Photochemical Transformations Accelerated in Continuous-flow Reactors: Basic Concepts and Applications. *Chemistry–A European Journal* **2014**, *20* (34), 10562–10589.
(21) Yagci, Y.; Tasdelen, M. A. Mechanistic Transformations Involving Living and Controlled/Living Polymerization Methods. *Prog Polym Sci* **2006**, *31* (12), 1133–1170.
(22) Chen, M.; Zhong, M.; Johnson, J. A. Light-Controlled Radical Polymerization: Mechanisms, Methods, and Applications. *Chem Rev* **2016**, *116* (17), 10167–10211.

(23) Corrigan, N.; Jung, K.; Moad, G.; Hawker, C. J.; Matyjaszewski, K.; Boyer, C. Reversible-Deactivation Radical Polymerization (Controlled/Living Radical Polymerization): From Discovery to Materials Design and Applications. *Prog Polym Sci* **2020**, *111*, 101311.

(24) Nwoko, T.; Watuthanthrige, N. D. A.; Parnitzke, B.; Yehl, K.; Konkolewicz, D. Tuning the Molecular Weight Distributions of Vinylketone-Based Polymers Using RAFT Photopolymerization and UV Photodegradation. *Polym Chem* **2021**, *12* (46), 6761–6770.

(25) Perrier, S. 50th Anniversary Perspective: RAFT Polymerization□ A User Guide. *Macromolecules* **2017**, *50* (19), 7433–7447.

(26) Golas, P. L.; Mueller, L. A.; Matyjaszewski, K. Fundamentals of Atom Transfer Radical Polymerization. *Encyclopedia of Polymer Science and Technology* **2002**.

(27) Tian, X.; Ding, J.; Zhang, B.; Qiu, F.; Zhuang, X.; Chen, Y. Recent Advances in RAFT Polymerization: Novel Initiation Mechanisms and Optoelectronic Applications. *Polymers (Basel)* **2018**, *10* (3), 318.

(28) Truong, N. P.; Jones, G. R.; Bradford, K. G. E.; Konkolewicz, D.; Anastasaki, A. A Comparison of RAFT and ATRP Methods for Controlled Radical Polymerization. *Nat Rev Chem* **2021**, *5* (12), 859–869.

(29) Shipp, D. A. Reversible-Deactivation Radical Polymerizations. *Polymer Reviews* **2011**, *51* (2), 99–103.

(30) Allegrezza, M. L.; DeMartini, Z. M.; Kloster, A. J.; Digby, Z. A.; Konkolewicz, D. Visible and Sunlight Driven RAFT Photopolymerization Accelerated by Amines: Kinetics and Mechanism. *Polym Chem* **2016**, *7* (43), 6626–6636.

(31) Parkatzidis, K.; Wang, H. S.; Truong, N. P.; Anastasaki, A. Recent Developments and Future Challenges in Controlled Radical Polymerization: A 2020 Update. *Chem* **2020**, *6* (7), 1575–1588.

(32) Bellotti, V.; Simonutti, R. New Light in Polymer Science: Photoinduced Reversible Addition-Fragmentation Chain Transfer Polymerization (PET-RAFT) as Innovative Strategy for the Synthesis of Advanced Materials. *Polymers (Basel)* **2021**, *13* (7), 1119.

(33) Zhou, J.; Sun, Y.; Huang, Z.; Luo, Z.; Hu, H. Improved Antifouling and Drug Delivery Properties of Polyvinyl Alcohol Hydrogel by Grafting with N-isopropylacrylamide via Organic Dye Photocatalyzed PET-RAFT Polymerization. *J Appl Polym Sci* **2021**, *138* (47), 51395.

(34) Hu, L.; Wang, Q.; Zhang, X.; Zhao, H.; Cui, Z.; Fu, P.; Liu, M.; Liu, N.; He, S.; Pang, X. Light and Magnetism Dual-Gated Photoinduced Electron Transfer-Reversible Addition–Fragmentation Chain Transfer (PET-RAFT) Polymerization. *RSC Adv* **2020**, *10* (12), 6850–6857.

(35) McClelland, K. P.; Clemons, T. D.; Stupp, S. I.; Weiss, E. A. Semiconductor Quantum Dots Are Efficient and Recyclable Photocatalysts for Aqueous PET-RAFT Polymerization. *ACS Macro Lett* **2019**, *9* (1), 7–13.

(36) Liang, Y.; Ma, H.; Zhang, W.; Cui, Z.; Fu, P.; Liu, M.; Qiao, X.; Pang, X. Size Effect of Semiconductor Quantum Dots as Photocatalysts for PET-RAFT Polymerization. *Polym Chem* **2020**, *11* (31), 4961–4967.

(37) Zhu, Y.; Liu, Y.; Miller, K. A.; Zhu, H.; Egap, E. Lead Halide Perovskite Nanocrystals as Photocatalysts for PET-RAFT Polymerization under Visible and near-Infrared Irradiation. *ACS Macro Lett* **2020**, *9* (5), 725–730.

(38) Zhu, Y.; Egap, E. PET-RAFT Polymerization Catalyzed by Cadmium Selenide Quantum Dots (QDs): Grafting-from QDs Photocatalysts to Make Polymer Nanocomposites. *Polym Chem* **2020**, *11* (5), 1018–1024.
(39) Yang, H.; Lu, Z.; Fu, X.; Li, Q.; Xiao, L.; Zhao, R.; Zhao, Y.; Hou, L. Multipath Oxygen-Mediated PET-RAFT Polymerization by a Conjugated Organic Polymer Photocatalyst under Red LED Irradiation. *Polym Chem* **2021**, *12* (48), 6998–7004.
(40) Satoh, K.; Sun, Z.; Uchiyama, M.; Kamigaito, M.; Xu, J.; Boyer, C. Interconvertible and Switchable Cationic/PET-RAFT Copolymerization Triggered by Visible Light. *Polym J* **2020**, *52* (1), 65–73.
(41) Ng, G.; Yeow, J.; Xu, J.; Boyer, C. Application of Oxygen Tolerant PET-RAFT to Polymerization-Induced Self-Assembly. *Polym Chem* **2017**, *8* (18), 2841–2851.
(42) Olson, R. A.; Korpusik, A. B.; Sumerlin, B. S. Enlightening Advances in Polymer Bioconjugate Chemistry: Light-Based Techniques for Grafting to and from Biomacromolecules. *Chem Sci* **2020**, *11* (20), 5142–5156.
(43) Li, M.; Fromel, M.; Ranaweera, D.; Rocha, S.; Boyer, C.; Pester, C. W. SI-PET-RAFT: Surface-Initiated Photoinduced Electron Transfer-Reversible Addition–Fragmentation Chain Transfer Polymerization. *ACS Macro Lett* **2019**, *8* (4), 374–380. https://doi.org/10.1021/acsmacrolett.9b00089.
(44) Zhang, Z.; Corrigan, N.; Bagheri, A.; Jin, J.; Boyer, C. A Versatile 3D and 4D Printing System through Photocontrolled RAFT Polymerization. *Angewandte Chemie International Edition* **2019**, *58* (50), 17954–17963. https://doi.org/https://doi.org/10.1002/anie.201912608.
(45) Moad, G.; Rizzardo, E. A 20th Anniversary Perspective on the Life of RAFT (RAFT Coming of Age). *Polym Int* **2020**, *69* (8), 658–661.
(46) Jiang, J.; Ye, G.; Wang, Z.; Lu, Y.; Chen, J.; Matyjaszewski, K. Heteroatom-doped Carbon Dots (CDs) as a Class of Metal-free Photocatalysts for PET-RAFT Polymerization under Visible Light and Sunlight. *Angewandte Chemie* **2018**, *130* (37), 12213–12218.
(47) Foster, H.; Stenzel, M. H.; Chapman, R. PET-RAFT Enables Efficient and Automated Multiblock Star Synthesis. *Macromolecules* **2022**.
(48) Li, J.; Wu, C.; Lei, Y.; Liu, W. Tuning Catalyst-Free Photocontrolled Polymerization by Substitution: A Quantitative and Qualitative Interpretation. *J Phys Chem Lett* **2022**, *13* (14), 3290–3296.
(49) Ng, G.; Yeow, J.; Chapman, R.; Isahak, N.; Wolvetang, E.; Cooper-White, J. J.; Boyer, C. Pushing the Limits of High Throughput PET-RAFT Polymerization. *Macromolecules* **2018**, *51* (19), 7600–7607.
(50) Phommalysack-Lovan, J.; Chu, Y.; Boyer, C.; Xu, J. PET-RAFT Polymerisation: Towards Green and Precision Polymer Manufacturing. *Chemical communications* **2018**, *54* (50), 6591–6606.
(51) Moad, G. RAFT Polymerization to Form Stimuli-Responsive Polymers. *Polym Chem* **2017**, *8* (1), 177–219.
(52) Kuhn, L. R.; Allegrezza, M. L.; Dougher, N. J.; Konkolewicz, D. Using Kinetic Modeling and Experimental Data to Evaluate Mechanisms in PET-RAFT. *Journal of Polymer Science* **2020**, *58* (1), 139–144.
(53) Theriot, J. C.; Miyake, G. M.; Boyer, C. A. N, N-Diaryl Dihydrophenazines as Photoredox Catalysts for PET-RAFT and Sequential PET-RAFT/O-ATRP. *ACS Macro Lett* **2018**, *7* (6), 662–666.

(54) Wong, A. M.; Valles, D. J.; Carbonell, C.; Chambers, C. L.; Rozenfeld, A. Y.; Aldasooky, R. W.; Braunschweig, A. B. Controlled-Height Brush Polymer Patterns via Surface-Initiated Thiol-Methacrylate Photopolymerizations. *ACS Macro Lett* **2019**, *8* (11), 1474–1478.
(55) Corrigan, N.; Xu, J.; Boyer, C.; Allonas, X. Exploration of the PET-RAFT Initiation Mechanism for Two Commonly Used Photocatalysts. *ChemPhotoChem* **2019**, *3* (11), 1193–1199. https://doi.org/https://doi.org/10.1002/cptc.201800182.
(56) Kurek, P. N.; Kloster, A. J.; Weaver, K. A.; Manahan, R.; Allegrezza, M. L.; de Alwis Watuthanthrige, N.; Boyer, C.; Reeves, J. A.; Konkolewicz, D. How Do Reaction and Reactor Conditions Affect Photoinduced Electron/Energy Transfer Reversible Addition–Fragmentation Transfer Polymerization? *Ind Eng Chem Res* **2018**, *57* (12), 4203–4213.
(57) Wilson, O. R.; Magenau, A. J. D. Oxygen Tolerant and Room Temperature RAFT through Alkylborane Initiation. *ACS Macro Lett* **2018**, *7* (3), 370–375.
(58) Zhao, B.; Li, J.; Xiu, Y.; Pan, X.; Zhang, Z.; Zhu, J. Xanthate-Based Photoiniferter RAFT Polymerization toward Oxygen-Tolerant and Rapid Living 3D Printing. *Macromolecules* **2022**, *55* (5), 1620–1628.
(59) Burridge, K. M.; de Alwis Watuthanthrige, N.; Payne, C.; Page, R. C.; Konkolewicz, D. Simple Polymerization through Oxygen at Reduced Volumes Using Oil and Water. *Journal of Polymer Science* **2021**, *59* (21), 2530–2536. https://doi.org/https://doi.org/10.1002/pol.20210386.
(60) Liarou, E.; Whitfield, R.; Anastasaki, A.; Engelis, N. G.; Jones, G. R.; Velonia, K.; Haddleton, D. M. Copper-Mediated Polymerization without External Deoxygenation or Oxygen Scavengers. *Angewandte Chemie International Edition* **2018**, *57* (29), 8998–9002. https://doi.org/https://doi.org/10.1002/anie.201804205.
(61) Allegrezza, M. L.; Konkolewicz, D. PET-RAFT Polymerization: Mechanistic Perspectives for Future Materials. *ACS Macro Lett* **2021**, *10* (4), 433–446.
(62) Kurek, P. N.; Kloster, A. J.; Weaver, K. A.; Manahan, R.; Allegrezza, M. L.; de Alwis Watuthanthrige, N.; Boyer, C.; Reeves, J. A.; Konkolewicz, D. How Do Reaction and Reactor Conditions Affect Photoinduced Electron/Energy Transfer Reversible Addition–Fragmentation Transfer Polymerization? *Ind Eng Chem Res* **2018**, *57* (12), 4203–4213.
(63) Craig, A. F.; Clark, E. E.; Sahu, I. D.; Zhang, R.; Frantz, N. D.; Al-Abdul-Wahid, M. S.; Dabney-Smith, C.; Konkolewicz, D.; Lorigan, G. A. Tuning the Size of Styrene-Maleic Acid Copolymer-Lipid Nanoparticles (SMALPs) Using RAFT Polymerization for Biophysical Studies. *Biochimica et Biophysica Acta (BBA) - Biomembranes* **2016**, *1858* (11), 2931–2939. https://doi.org/https://doi.org/10.1016/j.bbamem.2016.08.004.
(64) Reeves, J. A.; Allegrezza, M. L.; Konkolewicz, D. Rise and Fall: Poly (Phenyl Vinyl Ketone) Photopolymerization and Photodegradation under Visible and UV Radiation. *Macromol Rapid Commun* **2017**, *38* (13), 1600623.
(65) Reeves, J. A.; de Alwis Watuthanthrige, N.; Boyer, C.; Konkolewicz, D. Intrinsic and Catalyzed Photochemistry of Phenylvinylketone for Wavelength-Sensitive Controlled Polymerization. *ChemPhotoChem* **2019**, *3* (11), 1171–1179.
(66) Ashen-Garry, D.; Selke, M. Singlet Oxygen Generation by Cyclometalated Complexes and Applications. *Photochem Photobiol* **2014**, *90* (2), 257–274. https://doi.org/https://doi.org/10.1111/php.12211.
(67) Sifri, R. J.; Ma, Y.; Fors, B. P. Photoredox Catalysis in Photocontrolled Cationic Polymerizations of Vinyl Ethers. *Acc Chem Res* **2022**, 15535–15538.

(68) Holzer, W.; Penzkofer, A.; Tsuboi, T. Absorption and Emission Spectroscopic Characterization of Ir (Ppy) 3. *Chem Phys* **2005**, *308* (1–2), 93–102.
(69) Wang, H.; Liao, Q.; Fu, H.; Zeng, Y.; Jiang, Z.; Ma, J.; Yao, J. Ir (Ppy) 3 Phosphorescent Microrods and Nanowires: Promising Micro-Phosphors. *J Mater Chem* **2009**, *19* (1), 89–96.
(70) Gao, Z.; Wang, F.; Guo, K.; Wang, H.; Wei, B.; Xu, B. Carrier Transfer and Luminescence Characteristics of Concentration-Dependent Phosphorescent Ir (Ppy) 3 Doped CBP Film. *Opt Laser Technol* **2014**, *56*, 20–24.
(71) Xu, J.; Jung, K.; Boyer, C. Oxygen Tolerance Study of Photoinduced Electron Transfer–Reversible Addition–Fragmentation Chain Transfer (PET-RAFT) Polymerization Mediated by Ru (Bpy) 3Cl2. *Macromolecules* **2014**, *47* (13), 4217–4229.
(72) Xu, J.; Jung, K.; Corrigan, N. A.; Boyer, C. Aqueous Photoinduced Living/Controlled Polymerization: Tailoring for Bioconjugation. *Chem Sci* **2014**, *5* (9), 3568–3575.
(73) Bradford, K. G. E.; Petit, L. M.; Whitfield, R.; Anastasaki, A.; Barner-Kowollik, C.; Konkolewicz, D. Ubiquitous Nature of Rate Retardation in Reversible Addition–Fragmentation Chain Transfer Polymerization. *J Am Chem Soc* **2021**, *143* (42), 17769–17777.
(74) Wanasinghe, S. v; Sun, M.; Yehl, K.; Cuthbert, J.; Matyjaszewski, K.; Konkolewicz, D. PET-RAFT Increases Uniformity in Polymer Networks. *ACS Macro Lett* **2022**, *11* (9), 1156–1161.
(75) Xu, J.; Fu, C.; Shanmugam, S.; Hawker, C. J.; Moad, G.; Boyer, C. Synthesis of Discrete Oligomers by Sequential PET-RAFT Single-unit Monomer Insertion. *Angewandte Chemie International Edition* **2017**, *56* (29), 8376–8383.
(76) Fors, B. P.; Hawker, C. J. Control of a Living Radical Polymerization of Methacrylates by Light. *Angewandte Chemie International Edition* **2012**, *51* (35), 8850–8853. https://doi.org/https://doi.org/10.1002/anie.201203639.